Please refer to Supplementary Materials for experimental set-up and results

Analysis of a Single Photon, 2-Qubit Spatial Mode System: Implementing A Linear Polarization-Based Approach to Bell State Entanglement and Grover's Algorithm

Neha Chandran
Thomas Jefferson High School for Science and Technology
June 4, 2025

Please refer to Supplementary Materials for experimental set-up and results

Abstract

Our research proposes a novel method for photonic quantum computing using a single-photon, 2-qubit spatial mode system. By encoding qubits in the polarization states of individual spatial modes, we implement and analyze Bell State entanglement and Grover's algorithm. Experimentally, we will use a 405 nm pump laser with a diode controller and BBO crystal, along with a combination of alignment mirrors, waveplates, and beamsplitters from the ThorLabs quantum optics kit. Computationally, we will use Perceval, a Python-based linear optical quantum computing library. However, phase interferences introduced by the initial beam splitter operation, modeled as a "Black Box" operator, are shown to skew the measurement outcomes and influence the behavior of single-qubit gates. We mitigate these effects by balancing the circuit with Hadamard gates, effectively canceling extra phase contributions. Our approach enables us to construct a single photon controlled-NOT gate that achieves uniform Hong-Ou-Mandel (HOM) interference across all detectors. Our Bell State created with this gate successfully violates the Clauser-Horne-Shimony-Holt (CHSH) inequality. Expanding on this framework, we observe that Grover's algorithm finds the marked state with 100% accuracy using Perceval's noisy Strong Linear Optical Simulator (SLOS) and with 98.8% accuracy when random phase shifts are infused into the model. By training a simple linear regression model, we can predict the algorithm's accuracy for specific nonrandom phase shifts with a mean squared error (MSE) of 3.70e-05 and an R^2 of 0.904.

I Introduction

The dynamic use of photons as qubits allows for the integration of prior technology, such as fiber optics and quantum dots into quantum computing hardware. In comparison to superconducting Josephson junctions, photons have higher coherence rates and are able to transmit information at the speed of light. In terms of practicality and environmental considerations, photonic quantum computers do not require extreme temperatures to function or severe pulses of energy to perform gate operations, unlike their popular counterpart modalities like superconducting and ion-trap quantum computers. Photons' inherent resistance to noise and quantum decoherence makes photonic quantum computing a fault-tolerant modality. This is one of many advantages that photons provide, making this method highly scalable.

Bell state entanglement is a critical component of quantum communication protocols, as its properties enable information sharing between two parties. In this paper, we consider producing a similar effect with a single photon system, using a beam recombination technique similar to a Mach-Zehnder interferometer and Hong-Ou-Mandel interference with polarizing beam splitters.

II Materials

The interferometer circuit was produced both computationally and experimentally. We used Perceval, Quandela's open-source photonic quantum computing toolkit to test for indistinguishability. We then used

Please refer to Supplementary Materials for experimental set-up and results

IBM's quantum computing toolkit, Qiskit, to test for Bell inequalities. Both packages are integrated as Python libraries.

III Computational Basis

In this study, encoded qubits contain two distinct degrees of freedom: polarization and spatial modes. Most quantum computing protocols use polarized qubits, which refer to the direction of the wave. However, in order for single-photon entanglement to be possible, we consider encoding spatial modes in addition to polarization. Spatial modes describe the distribution of energy from the propagation of Gaussian beams through a transverse plane.

Below, we define how to represent the two polarization states associated with each spatial mode.

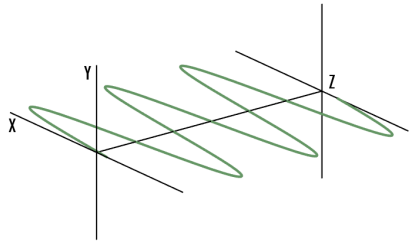

A. Horizontally polarized light

$$|0\rangle = \begin{bmatrix} 1 \\ 0 \end{bmatrix}$$

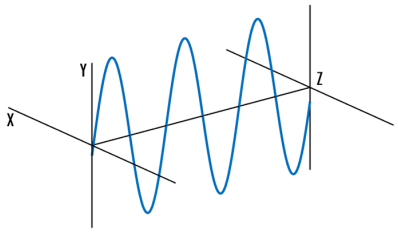

B. Vertically polarized light

$$|1\rangle = \begin{bmatrix} 0 \\ 1 \end{bmatrix}$$

In our experiment, the input photon's polarization begins in the form: $|\psi\rangle = |H\rangle$

IV Single Photon Path Entanglement

In this paper, we refer to the entanglement between spatial modes of a photon as single photon path entanglement. When the polarized photon passes through the first beam splitter, the Fock spaces for the two output modes are entangled. This effect is due to the photon being delocalized over multiple spatial locations simultaneously – analogous to the quantum mechanical definition of superposition.

Let's denote the two possible paths following the first beamsplitter as spatial mode A and spatial mode B. The state can then be represented as $|\psi\rangle = \alpha|A\rangle + \beta|B\rangle$, where α and β represent the probability amplitudes of the photon entering each path respectively.

Since we have a roughly 50-50 probability of entering either path, the state will look like,

$|\psi\rangle = \frac{1}{\sqrt{2}}|A\rangle + |B\rangle$. However, since we are treating each mode as an individual qubit, we can write the photon state as a two-qubit system using polarization.

Please refer to Supplementary Materials for experimental set-up and results

$$|\psi\rangle = |H\rangle_A \otimes |H\rangle_B = |HH\rangle$$

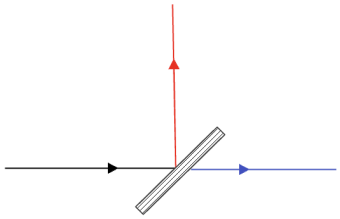

Figure 1: The black line represents the input photon, the red path represents spatial mode A, and the blue represents spatial mode B.

Our goal through the course of this paper will be to manipulate the spatial mode system such that the polarization state mirrors the third Bell state:

$$|\psi^+\rangle = \frac{1}{\sqrt{2}}|H\rangle_A + |V\rangle_A \otimes |V\rangle_B = \frac{1}{\sqrt{2}}(|HV\rangle + |VH\rangle)$$

V Adjusting for the Beamsplitter

The first step is to split the incoming photon into two modes using a beamsplitter in order to define the SPTQ system. However, we must be careful in using this operation, as the BS affects the behavior of waveplates and phase-shifters used to rotate the polarization of the spatial modes. For example, consider the effects on a toy model using a Pauli X-gate, which is represented as a half waveplate (lambda/2) rotated $\pi/4$ radians about the optical axis.

Below are the circuits in Perceval with and without the initial BS. Note modes 0 and 3 are ancilla qubits. Their purpose will be explained later with the actual model.

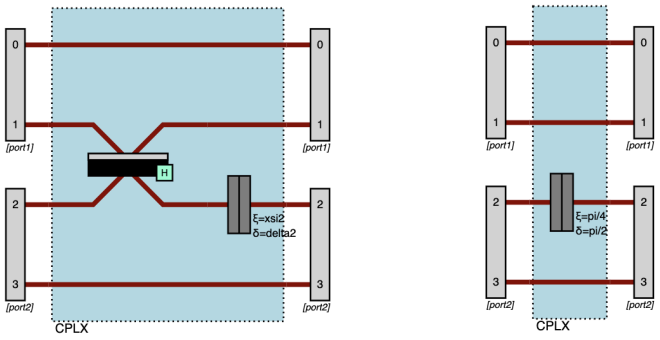

To visualize the photon coincidences at each detector, we can run a simulation in Perceval with 10,000 shots. We construct a processor using our circuit and the four detectors using two ports on spatial mode 0 and 2, as shown above. Then, we can define the input Fock state as $|0,1,0,0\rangle$ to fire a single photon

Please refer to Supplementary Materials for experimental set-up and results

through mode 1. Next, we add the input state to the processor and create a sampler object using the processor. The sampler is used to run 10,000 shots using the Linear Optical Simulator (SLOS) and the results are stored in a dictionary.

Below are the corresponding histograms for the toy models.

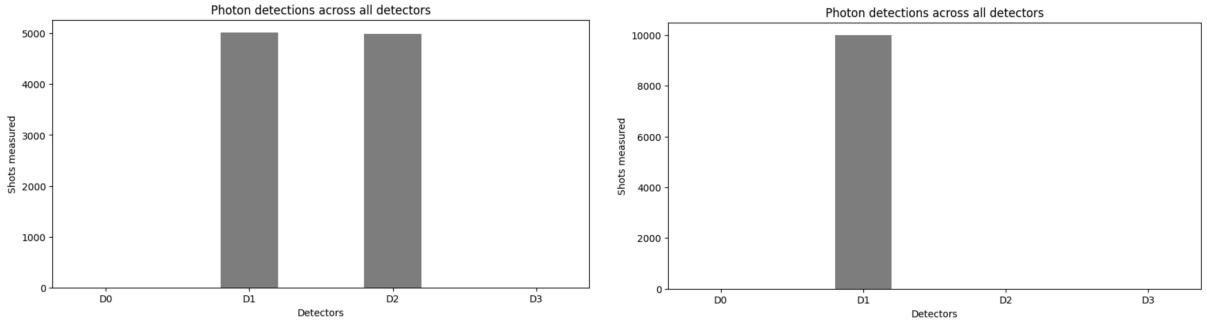

This clearly demonstrates the difference of including the beamsplitter to the system. In this model, a half waveplate cannot be linearly mapped to a Pauli X gate, but rather the combination of a Pauli X gate followed by a Hadamard gate.

Combining these operators into a single matrix, we can see that a bit-flip in our single photon, 2-qubit model can be represented as follows:

$$\begin{pmatrix} \frac{1}{\sqrt{2}} & -\frac{1}{\sqrt{2}} \\ \frac{1}{\sqrt{2}} & \frac{1}{\sqrt{2}} \end{pmatrix}$$

In Qiskit, this represented by the following circuit and probability distribution:

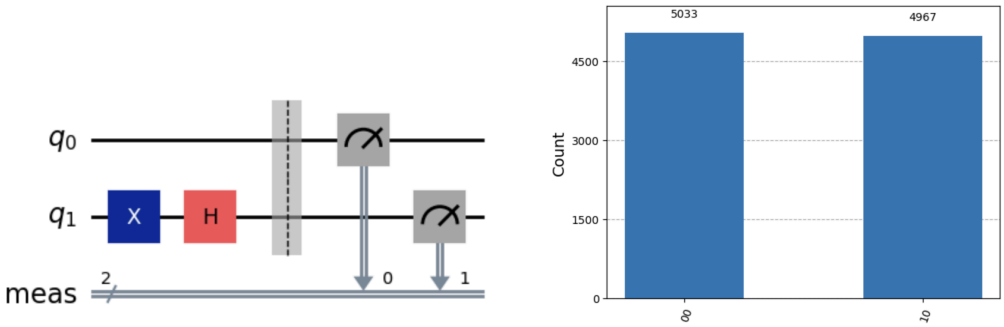

As shown, the probability distribution matches Fig Xa, as expected when the beamsplitter is in use.

To further understand the effects of the BS, consider its operator matrix notation given in Perceval's documentation:

Please refer to Supplementary Materials for experimental set-up and results

$$\begin{bmatrix} \cos(\theta/2) & \sin(\theta/2) \\ \sin(\theta/2) & -\cos(\theta/2) \end{bmatrix} \qquad \begin{bmatrix} 1 & 1 \\ 1 & -1 \end{bmatrix}$$

At a default value of theta = π/2, the beamsplitter behaves as a Hadamard gate in the spatial basis, effectively mixing the two paths such that the photon has a 50-50 probability in each state. However, as mentioned earlier, our experiment is focused on the polarization state evolution, rather than the spatial. From this standpoint, the initial beam splitter operation can be represented as a black box that introduces phase interferences and amplitude biases to the polarization states of the system. These interferences are complex and not directly measurable in the Perceval framework but are known to skew measurement distributions in entanglement circuits.

While this skew isn't easily visible in our toy model, its effects will be clear when constructing entanglement.

VI Part 1: Bell State Entanglement

Now that we have handled the nuances of the beamsplitter, we can construct entanglement in the |psi+> state. Accounting for the effects of the beamsplitter, the circuit in Qiskit is:

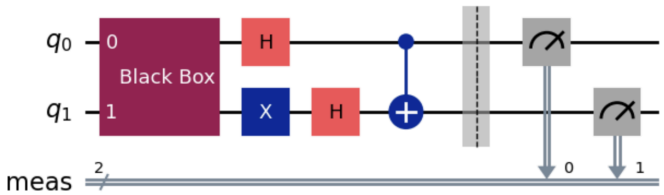

Where the Black Box operator and the second Hadamard gate correspond to the added contributions from the initial beamsplitter.

We can write the initial encoding as follows:

$$|\psi_a\rangle = \left(\frac{|0\rangle + |1\rangle}{\sqrt{2}} \langle 0| + \frac{|0\rangle - |1\rangle}{\sqrt{2}} \langle 1| \right) U_{\mathrm{BB}} |H\rangle$$

$$|\psi_b\rangle = \left(\frac{|0\rangle + |1\rangle}{\sqrt{2}} \langle 0| + \frac{|0\rangle - |1\rangle}{\sqrt{2}} \langle 1| \right) (|1\rangle \langle 1| + |0\rangle \langle 0| + |0\rangle \langle 1|) U_{\mathrm{BB}} |H\rangle$$

The *Part 1: Results and Discussion* section reveals the formal workings of this black box.

Please refer to Supplementary Materials for experimental set-up and results

To define this circuit in Perceval, we must initialize the polarization states of both spatial mode qubits. Initially, we defined that the bit flip operation corresponds to a half waveplate rotated π/4 radians. Drawing from past literature, the Hadamard operation corresponds to a half waveplate rotated π/8 radians.

Following our encoding, we will entangle the polarization states using the standard optical BSM procedure [5]. Kim et al. defines this procedure as two photons meeting and interfering at a BS. The paths are then passed through two polarizing beam splitters. We can extend this procedure to describe the overlap between two *spatial modes*.

This means that we must align the beams in such a way that they recombine at a second BS at the same time. To accomplish this, we set up a Mach-Zehnder interferometer scheme following our initial encoding.

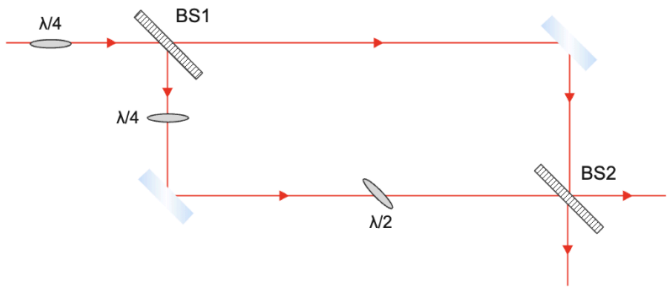

Fig. 2. MZI-inspired interference scheme. The input photon – represented by the incoming path – passes through a BS, producing spatial mode A – the upper path – and spatial mode B – the lower path. Similar to the real MZI, the two spatial modes recombine at the second BS.

Experimentally, some action must occur to construct the entangled state. The standard BSM procedure introduces two polarizing beam splitters (PBS) and involves a technique known as Hong-Ou-Mandel interference.

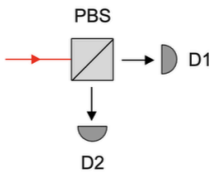

Fig. 3. HOM interference at a single PBS.

Traditionally, this effect occurs when two indistinguishable photons perfectly overlap at the PBS, causing them to exit from the same port 100% of the time. We consider extending this concept to two spatial modes as a verification of indistinguishability. Our research defines that each photon coincidence at the detector will correspond to perfectly overlapped spatial modes, indicating HOM interference. In an

Please refer to Supplementary Materials for experimental set-up and results

unbiased model, perfect indistinguishability required for entanglement corresponds to a roughly even distribution of photon coincidences. In other words, the modes are indistinguishable at every detector.

Therefore, our controlled-NOT gate in Perceval can be constructed as follows:

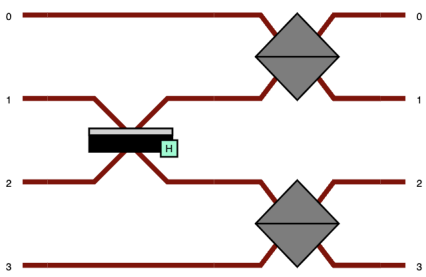

where modes 1 and 2 are the encoded spatial mode qubits, produced from the initial beamsplitter (not shown). This BS recombines the qubits and passes them to the PBS, where HOM interference takes place.

We now have all of the optical components to add to our interferometer in Perceval. The result is shown below.

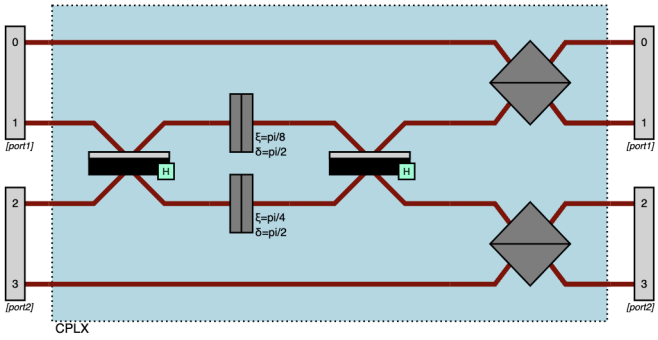

Fig. 4. Computer-generated circuit in Perceval where photon modes 1 and 2 encode the two qubits and modes 0 and 3 are ancillary, required for defining the four possible outcomes of measurement. The processor contains two ports (equivalent to four detectors). The photon is inputted through the D1 port..

Mathematically, the Hong-Ou-Mandel effect can be analyzed for a single photon, two mode system using Fock states and annihilation and creation operators[1].

$$\hat{a}^\dagger |0\rangle_a = \frac{1}{\sqrt{2}}(|0\rangle_a + |1\rangle_a) = |+\rangle_a$$

$$\hat{b}^\dagger |0\rangle_b = \frac{1}{\sqrt{2}}(|0\rangle_b + |1\rangle_b) = |+\rangle_b$$

which represents the photon in superposition of being present and non-present for both spatial modes a and b.

[1] In the spatial basis, not the polarization

Please refer to Supplementary Materials for experimental set-up and results

Combining the state, we get

$$|+,+\rangle_{ab} = \hat{a}^\dagger \hat{b}^\dagger |0,0\rangle_{ab}$$

Next, we can define our output modes *c* and *d*. When mixed at a 50:50 PBS, the probability of detection at our output modes are equal. Thus,

$$\hat{a}^\dagger = \frac{\hat{c}^\dagger + \hat{d}^\dagger}{\sqrt{2}}$$

$$\hat{b}^\dagger = \frac{\hat{c}^\dagger - \hat{d}^\dagger}{\sqrt{2}}$$

with a phase shift introduced from the beam-splitter for the output, given mode *b* as the input.

We can combine these two operations as follows,

$$|+,+\rangle_{ab} = \hat{a}^\dagger \hat{b}^\dagger |0,0\rangle_{ab} = \tfrac{1}{2}(\hat{c}^\dagger + \hat{d}^\dagger)(\hat{c}^\dagger - \hat{d}^\dagger) |+,+\rangle_{cd}$$

given that $\hat{c}^{\dagger 2} |+,+\rangle_{cd} = \sqrt{2} |1,0\rangle_{cd}$.

According to this result, when one photon is inputted as a superposition of modes *a* and *b*, the modes interfere at a beam splitter such that the qubits are bunched together at the outputs. The Fock state at each output mode is therefore taken out of superposition and represented as a single photon detection, corresponding to two spatial modes qubits.

As we did with the toy model, we can use Perceval's Strong Linear Optical Simulator (SLOS) to collect data and determine whether the modes are perfectly indistinguishable.

V Part 1: Results and Analysis

After running 10,000 shots, the photons are distributed across the detectors as follows.

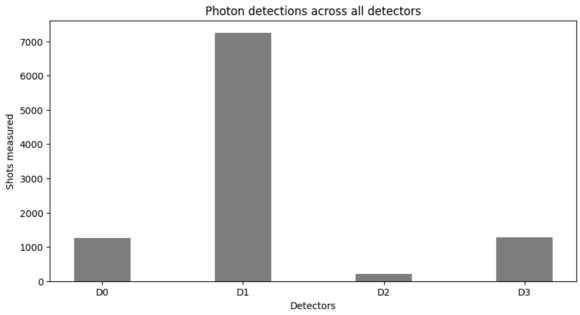

Please refer to Supplementary Materials for experimental set-up and results

At detector 1, we see a significantly higher proportion of photon detections, corresponding to indistinguishable, bunched spatial modes. However, the coincidences are much lower at the other detectors, indicating the spatial modes may not have perfectly overlapped at the second BS or at the PBS. Notice our results differ significantly from the expectation of uniformly distributed photon coincidences. This apparent skew in the distribution comes from the initial beamsplitter used to define our SPTQ system, as mentioned earlier. Now we can see clearly why in Qiskit we encapsulate this effect as a black box, yet cannot fully quantify its behavior due to the complexity of the system.

If we wanted to manually remove the bias from the system, we could add an additional half waveplate rotated π/8 radians after the half waveplate rotated π/4 radians. In Perceval, the circuit is given as:

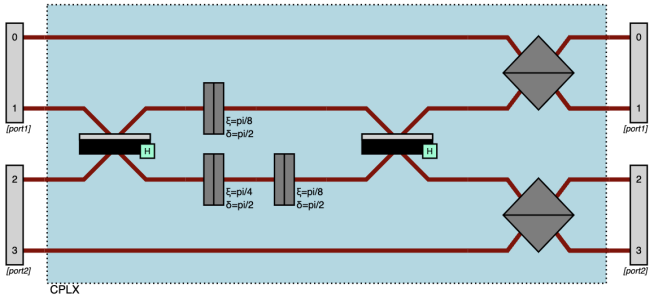

Then, using the SLOS simulator, the results are given below.

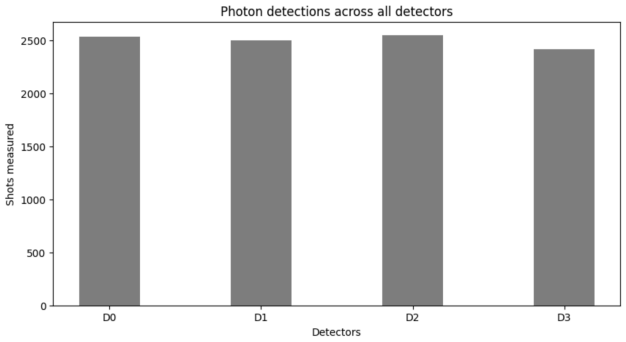

Fig. 5. Roughly uniform readings across all four detectors, indicating successful HOM interference as expected. Indistinguishable spatial mode qubits were “bunched” at each port.

We can contextualize these results by mapping to the following circuit in Qiskit.

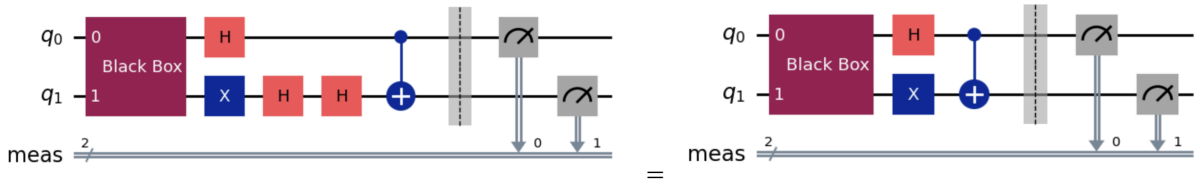

Please refer to Supplementary Materials for experimental set-up and results

Essentially, we are canceling out the extra Hadamard contribution present from the half waveplate rotated π/4 radians in the SPTQ system. Since our circuit is now balanced, the effects of the black box cancel out as well, leaving us with a symmetric, unskewed distribution as initially expected.

Thus, we can write the Black Box operation as follows:

$$U_{\text{BB}} = \begin{cases} I & \text{if the circuit is balanced} \\ U_{\text{skew}} & \text{if the circuit is imbalanced} \end{cases}$$

To further confirm our results, we consider rotating the angle of the half wave plate in eight π/4 radian increments about the optical axis and observing the changes in spatial mode indistinguishability. In other words, we are applying an RX gate. These findings can be summarized in the table below.

TABLE I
EXPECTED PHOTON COUNTS AT EACH DETECTOR GIVEN A WAVE-PLATE ROTATION OF ANY ANGLE.

Waveplate rotation across optical axis	**Photon coincidences at detector**
$\xi = 0 + k\pi, k \in \mathbb{Z}$	$\|0,0,0,1\rangle : 10000$
$\xi = 0 + \pi(2k-1)/4, k \in \mathbb{Z}$	$\|1,0,0,0\rangle : 2500$ $\|0,1,0,0\rangle : 2500$ $\|0,0,1,0\rangle : 2500$ $\|0,0,0,1\rangle : 2500$
$\xi = 0 + \pi(2k-1)/2, k \in \mathbb{Z}$	$\|1,0,0,0\rangle : 10000$

When the half-wave plate is rotated by angles in multiples of π, all photons are detected in the D3 detector, indicating unsuccessful HOM interference. When the angle is in multiples of π/4, we obtain roughly equal measurements across all four detectors, indicating successful interference. When the angle is in multiples of π/2, we see similar results to multiples of π, except all photons are now detected in the D0 detector. For a clearer visualization, refer to the figure below.

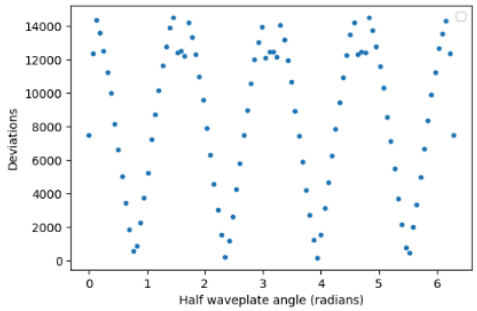

Fig. 6. Deviations from ideal count of 2500 photon detections per detector when the half wave plate is rotated by angles between $[0, 2\pi]$. Minimal deviations occur when $\xi = 0 + (2k-1)\pi/2, k \in \mathbb{Z}$

Please refer to Supplementary Materials for experimental set-up and results

This oscillatory behavior gels well with previous research to confirm entanglement in polarization-based photonics set-ups. In contrast, the biased model produces a deviations plot as follows:

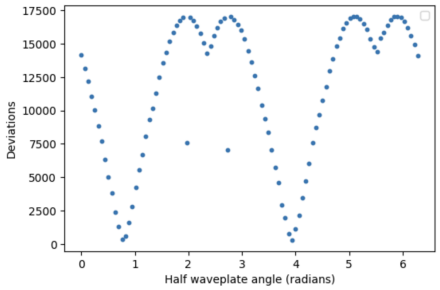

Deviations from ideal count of 1275-7250-200-7250 when the half wave plate is rotated by angles between [0, 2π]. This curve does not exhibit the same sinusoidal behavior as Fig X as a result of not eliminating the unique interference features of the initial beamsplitter.

At this point, we have rigorously confirmed HOM interference in the bias-mitigated model when $\xi = 0 + (2k - 1)\pi/2$, $k \in Z$, establishing the indistinguishability of the modes. This serves as a critical component of the standard Bell state measurement procedure, setting us apart from previous research in the field which simply calculates correlations between measurements of the modes' polarization states.

We, too, can calculate measurement correlations using the Clauser-Horne-Shimony-Holt inequality to confirm entanglement. The CHSH inequality is defined as follows:

$$\langle A_0 \otimes B_0 \rangle + \langle A_0 \otimes B_1 \rangle + \langle A_1 \otimes B_0 \rangle - \langle A_1 \otimes B_1 \rangle = 2\sqrt{2}$$

where A_0 and A_1 are the polarization bases for spatial mode A and B_0 and B_1 are the polarization bases for spatial mode B.

To change the measurement basis appropriately, we will rotate the Bell state around the Bloch sphere by an angle θ such that it produces the state:

$$|\psi\rangle = \frac{1}{\sqrt{2}}(\cos\theta/2\,|01\rangle + \sin\theta/2\,|10\rangle)$$

In Qiskit, this is effectively accomplished by applying an RY gate following the Bell state creation.

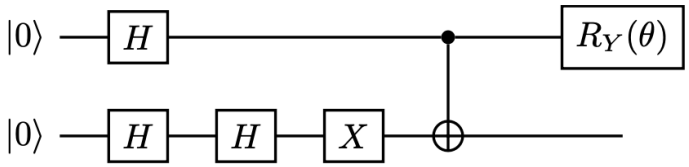

Once we execute the parameterization, we can plot the inequality bounds. Refer to the figure below for a visualization.

Please refer to Supplementary Materials for experimental set-up and results

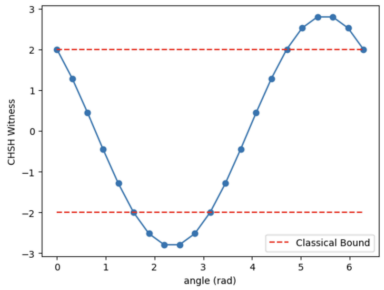

Fig. 7. CHSH inequality test using angles parameterized between [0,2π]. The inequality was successfully violated with |S| > 2 and |S| < 2, aligning with Tsirelson's bound, as indicated by the peaks above and below the red boundaries.

Therefore, we have successfully addressed the discrepancies in using the initial beamsplitter. Furthermore, by extending Kim et al's standard BSM procedure, we have provided an outline for constructing the controlled-NOT operation in our SPTQ system. We now have sufficient evidence demonstrating our spatial mode qubits are in this state:

$$|\psi\rangle = \frac{1}{\sqrt{2}}(|HV\rangle + |VH\rangle)$$

VI Part 2: Grover's Algorithm

Bell state entanglement is not the only operation that can be reproduced in our polarization-encoded SPTQ system. In fact, we can use the waveplates and the proposed controlled-NOT gate to implement much larger and powerful algorithms. In this section, we will outline the implementation for Grover's Algorithm and discuss its implications in our system.

Grover's algorithm begins by defining an initial guess state, expressed as a uniform superposition of the basis vectors as shown below:

$$|s\rangle = \frac{1}{\sqrt{N}} \sum_{x=0}^{N-1} |x\rangle$$

Where $|x\rangle$ is the general basis vector and N is the number of items in the dataset.

Our uniform superposition contains the state which we are searching for, which we can call $|w\rangle$. Let's define another state $|s'\rangle$ which removes $|w\rangle$ from $|s\rangle$. In other words,

$$\langle s'|w\rangle = 0$$

Please refer to Supplementary Materials for experimental set-up and results

Next, we need to define the *oracle* U_f, which operates on $|x\rangle$ as follows:

$$U_f |x\rangle = \begin{cases} -|x\rangle & \text{if } x \neq w \\ |x\rangle & \text{if } x = w \end{cases}$$

In effect, applying this operator will rotate $|s\rangle$ about $|s'\rangle$, flipping the sign of its amplitude. See the standard geometric visualization below.

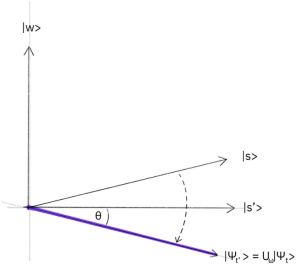

Then, we define the *diffuser* $U_s = 2|s\rangle\langle s| - I$ such that it rotates the state $U_f|x\rangle$ about $|s\rangle$. As shown below, the state $U_s U_f|x\rangle$ is now closer to $|w\rangle$.

For our 2-qubit system, there are $N = 4$ elements, and $|s\rangle$ is given as:

$$|s\rangle = \frac{1}{2}(|HH\rangle + |HV\rangle + |VH\rangle + |VV\rangle)$$

In our research, we marked the winning state as $|VH\rangle$.

Thus, the oracle, U_f, should rotate the state such that the sign of the $|VH\rangle$ component is flipped, yielding the new state:

$$|s\rangle = \frac{1}{2}(|HH\rangle + |HV\rangle - |VH\rangle + |VV\rangle)$$

Please refer to Supplementary Materials for experimental set-up and results

In Qiskit, this is accomplished by applying an X gate on the first qubit, followed by a controlled-phase gate, and another X gate.

The reflection portion of U_s can be evaluated by calculating the outer product as shown below.

$$U_s = 2 \cdot \tfrac{1}{2} \begin{pmatrix} 1 \\ 1 \\ 1 \\ 1 \end{pmatrix} \tfrac{1}{2} \begin{pmatrix} 1 & 1 & 1 & 1 \end{pmatrix} - I$$

In our Qiskit code, this is represented with H gates on both qubits 1 and 2, followed by Z gates on both qubits 1 and 2, followed by a CZ gate, and finally followed by H gates on both qubits 1 and 2 again.

However, when we implement this circuit in Perceval, the phase flip operation will include an extra Hadamard contribution, so we will need to account for this in our Qiskit code–similar to how we constructed $|\psi^+\rangle$. And of course, we will need our black box operation.

Putting each of these operations together, the final circuit in Qiskit will be as follows:

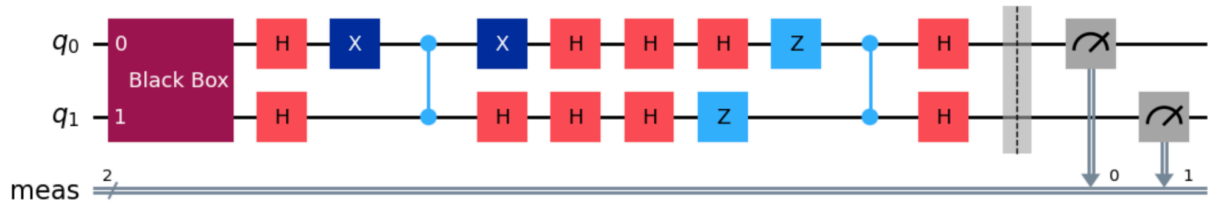

We can simplify this circuit to the one given below:

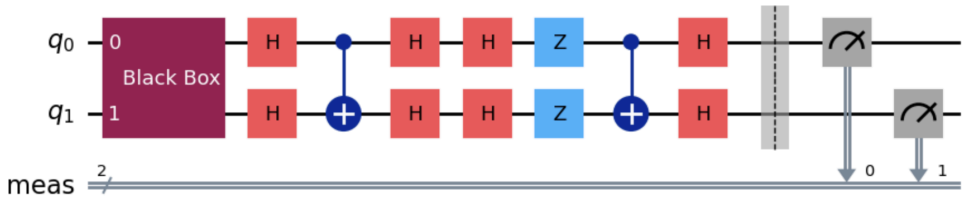

By replacing the CZ operations with CNOTs, we no longer needed to cancel out the extra Hadamard contributions from the Perceval phase shifter, reducing the overall number of components needed.

VII Part 2: Results and Analysis

When we run the circuit above using the Qiskit Aer simulation, our results match the |w> state we aimed to amplify. See below.

Please refer to Supplementary Materials for experimental set-up and results

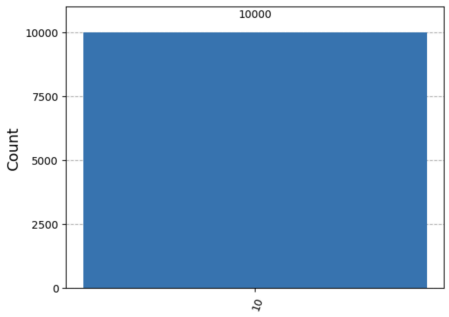

As we can see, this circuit has inherent symmetry, meaning the Black Box operation essentially behaves as an identity gate and does not skew the outcomes of measurement.

Now that we've simplified the circuit and taken care of bias, we can easily map these results to Perceval, making use of the fact that the Z gate in Perceval is a π-phase shifter.

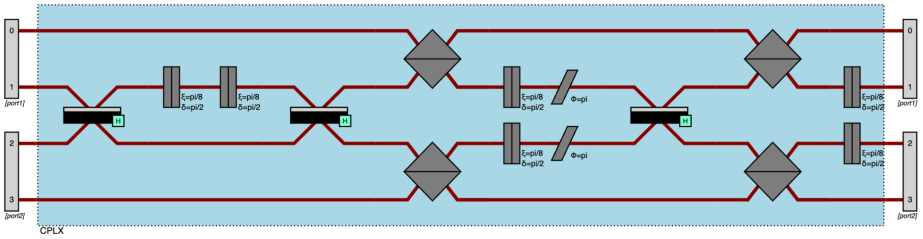

Using the Strong Linear Optical Simulator, the photon coincidences are given below:

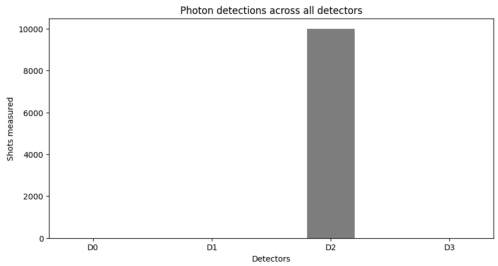

These results match our Qiskit simulation, as the spatial mode qubits were detected in a single state (|w>) at detector 2. Therefore, Grover's algorithm was implemented successfully.

As we did with the Bell State creation, we can contextualize our results from the perspective of Hong-Ou-Mandel interference. For maximum entanglement, we expect to observe perfect indistinguishability across all four detectors. On the other hand, the histogram for Grover's shows the spatial modes are only indistinguishable at detector 2.

This makes sense because we expect Grover's to have high distinguishability. This translates well to the CHSH inequality. If we parameterize our Grover's circuit as we did with the Bell circuit, the results are given below.

Please refer to Supplementary Materials for experimental set-up and results

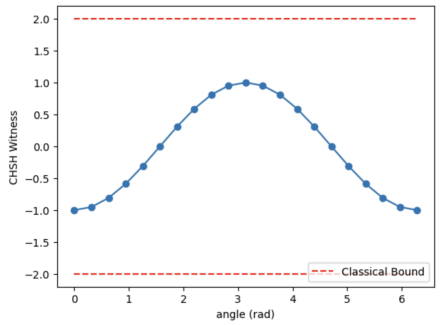

The high distinguishability in the system prevents the Tsierelson bounds from being violated. Conceptually, this makes sense, as we do not expect to create an entangled state when executing Grover's.

Returning to our Perceval model, we can create a more accurate simulation by infusing noise into our circuit.

Because the Perceval framework doesn't include built-in customizable noise models, we can manually simulate noise by adding random phase shifters at different points in the circuit. To match realistic photonic NISQ devices, we will define the amount of phase shift as follows:

```
def random_phase_shift():

    return np.random.uniform(0, np.pi/6)
```

For consistency, we will apply these phase shifters on all four modes (qubits A and B, as well as the two ancilla modes).

Below is a table of results from the new simulation:

Step	**State (Counts)**
Start	$\{ \|0,0,1,0\rangle$: 10000 $\}$
After initial BS (the black box)	$\{ \|0,1,0,0\rangle$: 459, $\|0,0,1,0\rangle$: 9541 $\}$
After first set of HWPs rotated $\pi/8$ rads (Hadamard gate)	$\{ \|0,1,0,0\rangle$: 2, $\|0,0,1,0\rangle$: 9998 $\}$
After second BS + 2 PBS (CNOT gate)	$\{ \|0,0,1,0\rangle$: 10000 $\}$
After second set of HWPs rotated $\pi/8$ rads	$\{ \|0,0,1,0\rangle$: 10000 $\}$
After first set of π-phase shifters (Z gate followed by Hadamard)	$\{ \|0,0,1,0\rangle$: 10000 $\}$
After third BS + 2 PBS (second CNOT gate)	$\{ \|0,0,1,0\rangle$: 10000 $\}$
After third set of HWPs rotated $\pi/8$ rads	$\{ \|0,0,1,0\rangle$: 10000 $\}$

As we can see, at most points, our circuit is inherently noise resistant. However, after the initial beamsplitter, we see the most deviation from the perfect 100% detection of the marked state. To find the true noisy probability of detecting the marked state, we can run 10 trials with random noise at this point, measure the photon coincidences as we did in the table above, and calculate the average.

Please refer to Supplementary Materials for experimental set-up and results

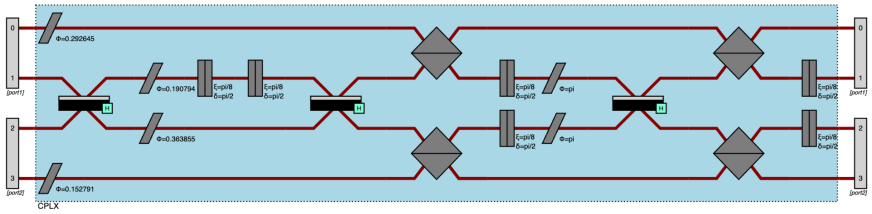

Example of said circuit. The first four phase shifters are the infusion of noise.

Based on our data, we can calculate the average number of photon coincidences, yielding a 98.765% probability of detecting the marked state $|VH\rangle$.

To obtain a more comprehensive view, we constructed and trained a simple linear regression machine learning model to predict the accuracy of Grover's algorithm under variant phase noise. See the scatterplots below implementing the model in Perceval *(left)* and Qiskit *(right)*.

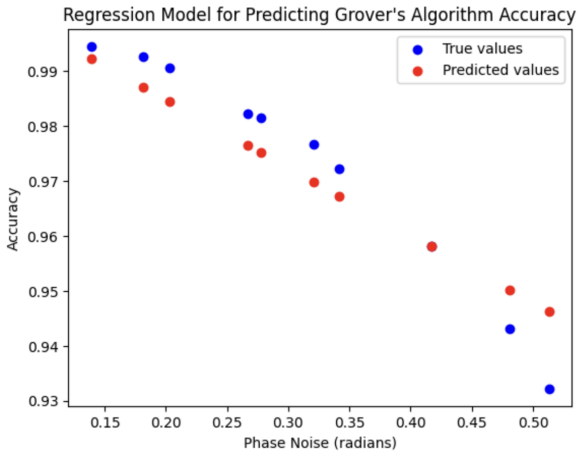

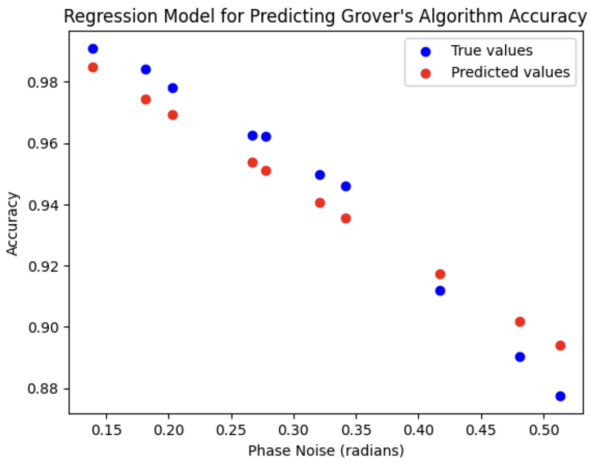

In Perceval, we obtain a mean squared error (MSE) of 4.65e-05 and an R^2 of 0.887. In Qiskit, we obtain a mean squared error (MSE) of 1.04e-04 and an R^2 of 0.926.

VIII Conclusion

The results above align with the possibility of producing entanglement within a single photon by encoding the qubits as spatial modes.

In effect, for certain quantum communications protocols, we could linearly reduce the number of photons required. As an example, the E91 quantum key distribution protocol, proposed by Artur Ekert in 1991, securely transfers information between an entangled pair. Traditionally, this requires two photons, but by

Please refer to Supplementary Materials for experimental set-up and results

encoding the polarization bases in the protocol spatial modes, the effect can be replicated using a single photon, 2-qubit system.

For the diagonal basis, we define $|A\rangle$ and $|D\rangle$ to represent our orthogonal pair between the modes, where:

$$|H\rangle = \frac{1}{\sqrt{2}}(|D\rangle + |A\rangle)$$
$$|V\rangle = \frac{1}{\sqrt{2}}(|D\rangle - |A\rangle)$$

Then the entangled state becomes:

$$|\psi\rangle^+ = \frac{1}{2\sqrt{2}}(|D\rangle_A + |A\rangle_A)(|D\rangle_B + |A\rangle_B) + (|D\rangle_A - |A\rangle_A)(|D\rangle_B + |A\rangle_B)$$

which simplest to:

$$|\psi\rangle^+ = \frac{1}{2\sqrt{2}}\,|A\rangle_A\,|D\rangle_B + |D\rangle_A\,|A\rangle_B$$

In theory, the schematic can be extended to systems with > 2 modes and higher degrees of freedom, opening a realm of possibilities. However, the precise alignment of advanced tools such as diffractive beamsplitters (DOE), capable of splitting an incoming beam into n modes, presents a challenge. Looking forward, this fundamental change in encoding, as suggested by our project, could transform the way quantum communications systems work today, leading to groundbreaking innovations in the field.

IX References

Biswas, K. K., & Sajeed, S. (2012). Design and realization of a quantum Controlled NOT gate using optical implementation. International Journal of Advancements in Research & Technology, 1(1), 20-28.

Caspar, P., Verbanis, E., Oudot, E., Maring, N., Samara, F., Caloz, M., Perrenoud, M., Sekatski, P., Martin, A., Sangouard, N., Zbinden, H., & Thew, R. (2020). Heralded distribution of single-photon path entanglement. Physical Review Letters, 125(11). https://doi.org/10.1103/physrevlett.125.110506

Please refer to Supplementary Materials for experimental set-up and results

Fiorentino, M., & Wong, F. (2004). Deterministic controlled-not gate for single-photon two-qubit quantum logic. Physical Review Letters, 93(7). https://doi.org/10.1103/physrevlett.93.070502

Kim, Y., Pramanik, T., Cho, Y., Yang, M., Han, S., Lee, S., Kang, M., & Moon, S. (2018). Informationally symmetrical Bell state preparation and measurement. Optics Express, 26(22), 29539-29549. https://doi.org/10.1364/OE.26.029539

Mohan, N.K., Bhowmick, R., Kumar, D., & Chaurasiya, R. (2024). Digital quantum simulations of Hong-Ou-Mandel interference, ArXiv, https://arxiv.org/pdf/2301.12505.pdf.

Shafi, K. M., Gayatri, R., Padhye, A., & Chandrashekar, C. M. (2021). Bell-inequality in path-entangled single photon and purity test.

Zeuner, J., Sharma, A. N., Tillmann, M., Heilmann, R., Gräfe, M., Moqanaki, A., Szameit, A., & Walther, P. (2018). Integrated-optics heralded controlled-NOT gate for polarization-encoded qubits. npj Quantum Information, 4(1), 1-7. https://doi.org/10.1038/s41534-018-0068-0